The Theory of Characteristic Modes Revisited: A Contribution to the Design of Antennas for Modern Applications

Marta Cabedo-Fabrés, Eva Antonino-Daviu, Alejandro Valero-Nogueira and Miguel Ferrando Bataller

Universidad Politécnica de Valencia, Departamento de Comunicaciones
Camino de Vera s/n, 46022, Valencia, Spain
Tel: +34 963879584
E-mail: marcafab@dcom.upv.es; evanda@upvnet.upv.es; avalero@dcom.upv.es; mferrand@dcom.upv.es

Abstract

The objective of this paper is to summarize the work that has been developed by the authors for the last several years, in order to demonstrate that the Theory of Characteristic Modes can be used to perform a systematic design of different types of antennas. Characteristic modes are real current modes that can be computed numerically for conducting bodies of arbitrary shape. Since characteristic modes form a set of orthogonal functions, they can be used to expand the total current on the surface of the body. However, this paper shows that what makes characteristic modes really attractive for antenna design is the physical insight they bring into the radiating phenomena taking place in the antenna. The resonance frequency of modes, as well as their radiating behavior, can be determined from the information provided by the eigenvalues associated with the characteristic modes. Moreover, by studying the current distribution of modes, an optimum feeding arrangement can be found in order to obtain the desired radiating behavior.

Keywords: Antenna theory; numerical analysis; optimization methods; eigenvalues and eigenfunctions; broadband antennas; antenna feeds; microstrip antennas; monopole antennas; land mobile radio cellular equipment; handset antennas; reflectarray

1. Introduction

In past years, the rise of wireless communications has fostered significant interest in antenna design. In particular, the design of small antennas for new mobile terminals [1, 2] is currently receiving a lot of attention, due to market demand. Nevertheless, designing a handset antenna is not an easy task, as this type of antenna is subject to very stringent specifications [3]. Small size, light weight, compact structure, low profile, robustness, and flexibility are the prime considerations conventionally taken into account in small-antenna design [4]. In addition, as new mobile handsets are required to operate with multiple standards, their antennas are expected to grab as much spectrum as possible, so they may provide multi-band or broadband operation [5].

Unfortunately, as the antenna geometry becomes more complicated, more often than not there is no closed formulation to analyze it, and the use of numerical methods [6, 7] becomes imperative. As a consequence, the design of modern handset antennas relies on the use of self-developed numerical codes or commercial electromagnetic simulators – such as *IE3D*, *FEKO*, *Empire*, or *HFSS*, among others – to evaluate antenna performance before a physical prototype is fabricated. Under these circumstances, the time required for antenna design can be dramatically reduced using computers. Even with the support of computers, the success of the final design depends upon the intuition and previous experience of the designer. In most cases, the final optimization is in fact made by "cut and try" methods. As a result, these days antenna design is very much governed by designer expertise and know-how.

On the other hand, an alternative and a certainly in-vogue approach for designing handset antennas consists of using automated optimization techniques, based on pseudo-random search algorithms [8]. Typical examples of these techniques are genetic algorithms [9], artificial neural networks [10], particle-swarm optimization [11], or bees algorithms [12]. The main advantage of these methods is that once the optimization algorithm is programmed, little interaction with the designer is required, as the computer is supposed to arrive at the expected specifications autonomously.

As a matter of fact, although all the above-mentioned design strategies are really suitable when time-to-market is critical, their major problem is that they are rather lacking in physical insight, so real knowledge of the antenna operating principles is mislaid. Consequently, publications giving useful instructions for better antenna design are scarce. There exist other not-so-common design strategies, such as the Theory of Characteristic Modes, which can alleviate this problem.

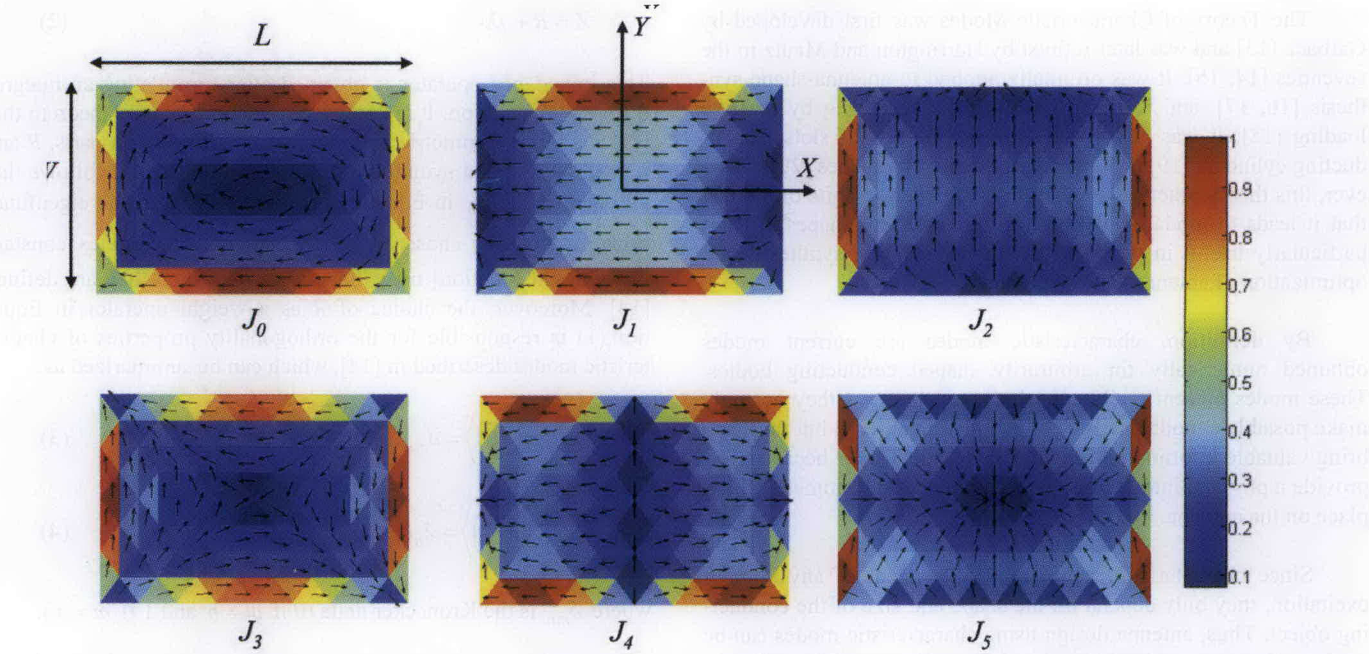

Figure 1. The normalized current distributions at the first resonance ($f = 2.4$ GHz) of the first six eigenvectors, J_n, of a rectangular plate of width $W = 4$ cm and length $L = 6$ cm.

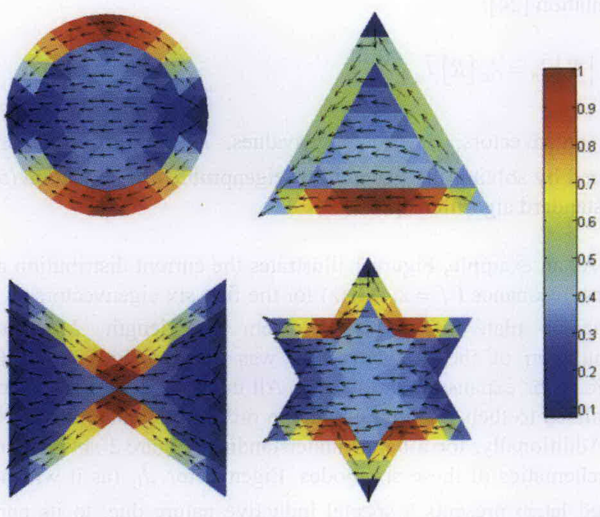

Figure 7a. The normalized current distribution of the horizontal current mode (J_1) at 2.4 GHz of the first eigenvectors of several planar geometries.

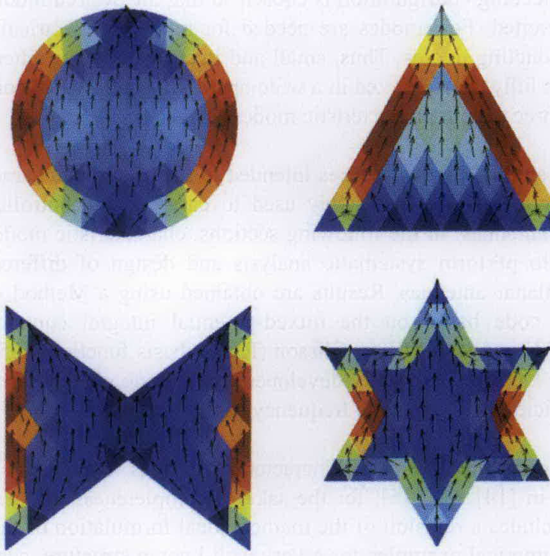

Figure 7b. The normalized current distribution of the vertical current mode (J_2) at 2.4 GHz of the first eigenvectors of several planar geometries.

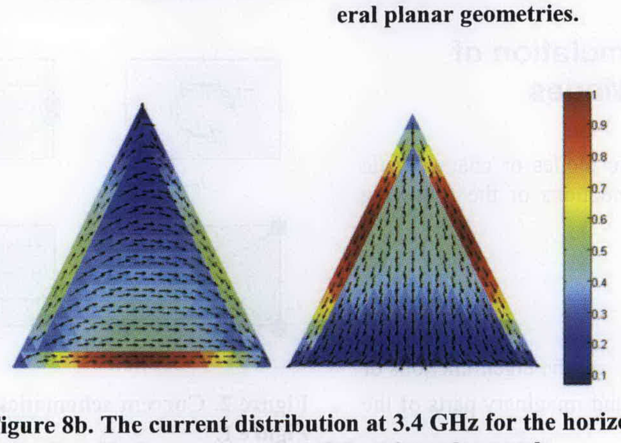

Figure 8b. The current distribution at 3.4 GHz for the horizontal and vertical current modes of the triangular patch.

The Theory of Characteristic Modes was first developed by Garbacz [13] and was later refined by Harrington and Mautz in the seventies [14, 15]. It was originally applied to antenna-shape synthesis [16, 17], and to control of obstacle scattering by reactive loading [18]. It was also applied to the analysis of slots in conducting cylinders [19] or in perfectly conducting planes [20]. However, this theory practically fell into disuse later, in spite of the fact that it leads to modal solutions even for arbitrary shapes. This is particularly useful in problems involving analysis, synthesis, and optimization of antennas and scatterers [21-23].

By definition, characteristic modes are current modes obtained numerically for arbitrarily shaped conducting bodies. These modes present really appealing properties, as they not only make possible a modal analysis of conducting objects, but they also bring valuable information for antenna design. This is because they provide a physical interpretation of the radiation phenomena taking place on the antenna.

Since characteristic modes are independent of any kind of excitation, they only depend on the shape and size of the conducting object. Thus, antenna design using characteristic modes can be performed in two steps. First, the shape and size of the radiating element are optimized. If the size of the element is scaled, the resonant frequency of the modes will be modified, whereas if the shape of the element is varied, not only the resonant frequency but also the radiating properties of the modes will change. Next, the optimum feeding configuration is chosen so that the desired modes may be excited. Few modes are needed for modeling electrically small conducting bodies. Thus, small and intermediate-size antennas can be fully characterized in a wide operating band by just considering three or four characteristic modes.

The study presented here is intended to illustrate that characteristic modes can be effectively used to carry out a controlled design of antennas. In the following sections, characteristic modes are used to perform systematic analysis and design of different types of planar antennas. Results are obtained using a Method of Moments code based on the mixed-potential integral equation (MPIE) [24] and Rao-Wilton-Glisson (RWG) basis functions [25]. This code has been expressly developed to compute characteristic modes efficiently over a wide frequency band.

Although the Theory of Characteristic Modes is extensively described in [14] and [15], for the sake of completeness the next section includes a revision of the mathematical formulation of this theory. Numerical examples for a very well-known structure, such as a rectangular plate, are presented for illustration purposes.

2. Mathematical Formulation of Characteristic Modes

As explained in [14], characteristic modes or characteristic currents can be obtained as the eigenfunctions of the following particular weighted eigenvalue equation:

$$X\left(\vec{J}_n\right)=\lambda_n R\left(\vec{J}_n\right), \tag{1}$$

where the λ_n are the eigenvalues, the $\vec{J}_n$ are the eigenfunctions or eigencurrents, and R and X are the real and imaginary parts of the impedance operator

$$Z = R + jX . \tag{2}$$

This impedance operator is obtained after formulating an integro-differential equation. It is known from the reciprocity theorem that if Z is a linear symmetric operator, then, its Hermitian parts, R and X, will be real and symmetric operators. From this, it follows that all eigenvalues λ_n in Equation (1) are real, and all the eigenfunctions, $\vec{J}_n$, can be chosen real or equiphasal [a complex constant times a real function] over the surface on which they are defined [14]. Moreover, the choice of R as a weight operator in Equation (1) is responsible for the orthogonality properties of characteristic modes described in [14], which can be summarized as

$$\left\langle \overrightarrow{J_m^*}, R\left(\overrightarrow{J_n}\right)\right\rangle = \delta_{mn}, \tag{3}$$

$$\left\langle \overrightarrow{J_m^*}, X\left(\overrightarrow{J_n}\right)\right\rangle = \lambda_n \delta_{mn}, \tag{4}$$

where δ_{mn} is the Kronecker delta (0 if $m \neq n$ and 1 if $m = n$).

Consistent with Equation (1), the characteristic modes $\vec{J}_n$ can be defined as the real currents on the surface of a conducting body that only depend on its shape and size, and are independent of any specific source or excitation. In practice, to compute characteristic modes of a particular conducting body, Equation (1) needs to be reduced to matrix form, as explained in [15], using a Galerkin formulation [24]:

$$[X]\vec{J}_n = \lambda_n [R]\vec{J}_n . \tag{5}$$

Next, eigenvectors, $\vec{J}_n$, and eigenvalues, λ_n, of the object are obtained by solving the generalized eigenproblem of Equation (5) with standard algorithms [26].

As an example, Figure 1 illustrates the current distribution at the first resonance ($f = 2.4$ GHz) for the first six eigenvectors of a rectangular plate of width $W = 4$ cm and length $L = 6$ cm. Computation of these eigenvectors was done using 128 RWG functions for expansion and testing. All currents in Figure 1 were normalized to their maximum value in order to facilitate comparison. Additionally, for a better understanding, Figure 2 shows current schematics of these six modes. Eigenvector J_0 (as it will be verified later) presents a special inductive nature due, to its currents forming closed loops over the plate. Eigenvectors J_1 and J_2, which are characterized by horizontal and vertical currents, respec-

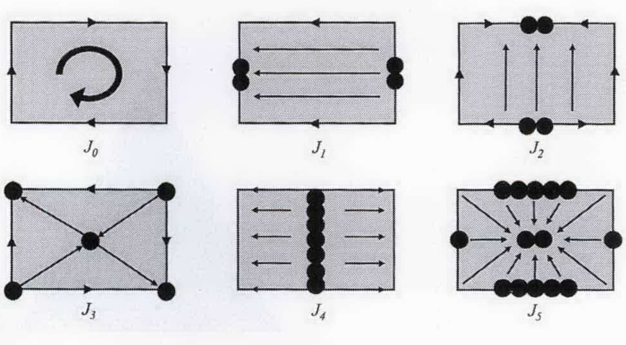

Figure 2. Current schematics for the six eigenvectors shown in Figure 1.

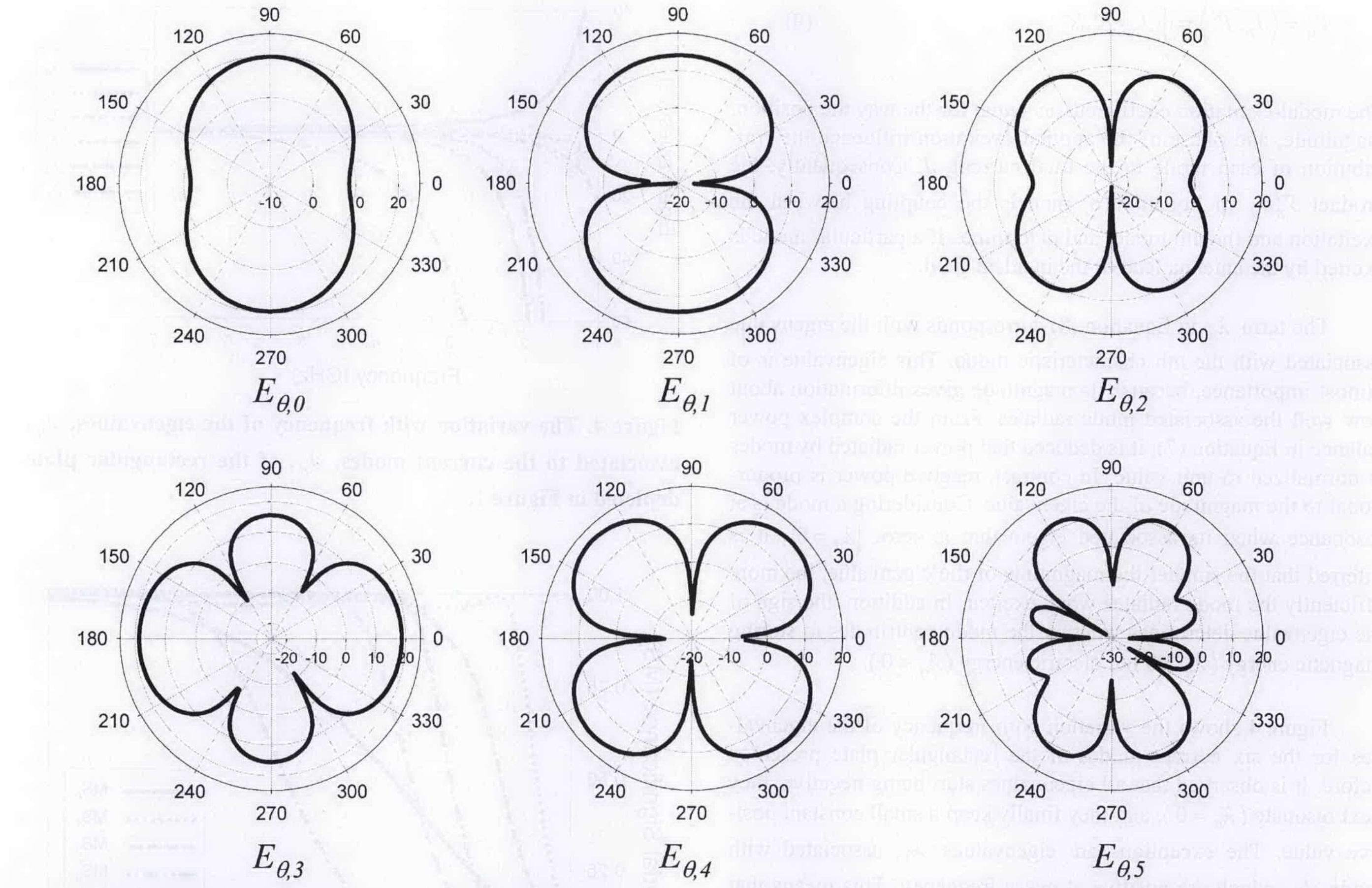

Figure 3. The azimuthal radiation pattern ($\theta = 90°$) at 4 GHz of the modal electric fields, $E_{\theta,n}$, produced by the current modes, J_n, of Figure 1.

tively, are the most frequently used modes in patch-antenna applications, while the rest of the eigenvectors, J_3, J_4, and J_5, are higher-order modes that might be taken into consideration only at the highest frequencies.

It is worth noting that the eigenvectors presented in Figure 1 were computed in free space. However, the presence of a ground plane below the plate would not significantly alter their current distribution, although it would affect their resonance and radiating bandwidth [27]. Note also that due to the eigenvectors' dependency upon frequency, if a structure is to be analyzed in a frequency range, modes will need to be recalculated at every frequency [28].

On the other hand, electric fields, E_n, produced by characteristic currents J_n on the surface of the conducting body are called characteristic fields [14]. From Equation (1), it can be derived that these characteristic fields can be written as

$$E_n\left(\vec{J}_n\right) = Z\left(\vec{J}_n\right) = R\left(\vec{J}_n\right) + jX\left(\vec{J}_n\right) = R\left(\vec{J}_n\right)\left(1 + j\lambda_n\right). \tag{6}$$

Then, from Equation (6), it is deduced that characteristic electric fields are equiphasal, since they are $(1 + j\lambda_n)$ times a real quantity. Orthogonality relationships for characteristic electric fields can be reached from characteristic currents by means of the complex Poynting theorem:

$$P\left(J_m, J_n\right) = \left\langle J_m^*, ZJ_n\right\rangle = \left\langle J_m^*, RJ_n\right\rangle + j\left\langle J_m^*, XJ_n\right\rangle$$
$$= \oint\!\!\!\oint_{S'} \vec{E}_m \times \vec{H}_n^* ds + j\omega \iiint_{\tau'} \left(\mu \vec{H}_m \bullet \vec{H}_n^* - \varepsilon \vec{E}_m \bullet \vec{E}_n^*\right) d\tau$$
$$= \left(1 + j\lambda_n\right)\delta_{mn}. \tag{7}$$

Figure 3 depicts the azimuthal radiation pattern ($\theta = 90°$) at 4 GHz for the modal electric fields, E_n, produced by the current modes, J_n, of the rectangular plate. It can be observed that the radiation pattern generated by mode J_0 presents a nearly omnidirectional characteristic, while the rest of modes present a growing number of lobes as the order of the mode increases.

Due to the above-mentioned orthogonality properties over both the surface of the body and the enclosing sphere at infinity, characteristic modes radiate power independently of one another. Because of this attractive feature, characteristic modes can be used as a basis set in which to expand the unknown total current, J, on the surface of the conducting body as

$$J = \sum_n \frac{V_n^i J_n}{1 + j\lambda_n} \tag{8}$$

The term V_n^i in Equation (8) is called the modal-excitation coefficient [14], and it is defined as

$$V_n^i = \langle J_n, E^i \rangle = \oint_n J_n \bullet E^i ds. \quad (9)$$

The modal-excitation coefficient accounts for the way the position, magnitude, and phase of the applied excitation influence the contribution of each mode to the total current, *J*. Consequently, the product $V_n^i J_n$ in Equation (8) models the coupling between the excitation and the *n*th mode, and determines if a particular mode is excited by the antenna feed or the incident field.

The term λ_n in Equation (8) corresponds with the eigenvalue associated with the *n*th characteristic mode. This eigenvalue is of utmost importance, because its magnitude gives information about how well the associated mode radiates. From the complex power balance in Equation (7), it is deduced that power radiated by modes is normalized to unit value. In contrast, reactive power is proportional to the magnitude of the eigenvalue. Considering a mode is at resonance when its associated eigenvalue is zero, $|\lambda_n = 0|$, it is inferred that the smaller the magnitude of the eigenvalue, the more efficiently the mode radiates when excited. In addition, the sign of the eigenvalue determines whether the mode contributes to storing magnetic energy ($\lambda_n > 0$) or electric energy ($\lambda_n < 0$).

Figure 4 shows the variation with frequency of the eigenvalues for the six current modes of the rectangular plate presented before. It is observed that all eigenvalues start being negative, they next resonate ($\lambda_n = 0$), and they finally keep a small constant positive value. The exceptions are eigenvalues λ_0, associated with mode J_0, which are positive at every frequency. This means that mode J_0, inherent in planar structures and wire loops, exhibits special behavior, as it does not resonate. If this mode were excited, it would only contribute to an increase in magnetic reactive power. For the particular case of the rectangular plate, as eigenvalues continue with very small values after resonance, it is difficult to identify where each curve passes though zero, and hence at which frequency each mode resonates.

Finally, it is worth mentioning that the real nature of characteristic modes derived from Equation (1) constitutes an advantage in comparison with complex natural modes directly obtained from impedance matrix $[Z]$. Working with complex basis functions leads to an increase in the complexity of computation, since it is necessary to give different treatment to the real and imaginary parts of the current to get accurate results [29]. Another drawback of natural modes is that their eigenvalues are also complex, and they thus are not so easy to analyze and explain physically. The next section explains in detail how to make the most of the information provided by eigenvalues to perform a complete modal characterization of an antenna.

3. Physical Interpretation of Characteristic Modes

As exposed before, an analysis of the eigenvalue variation with frequency is very useful for antenna design, as it brings information about the resonance and the radiating properties of the current modes. Nevertheless, in practice, other alternative representations of the eigenvalues are preferred.

Since the modal expansion of the current described in Equation (8) is inversely dependent upon the eigenvalues, it seems more consistent to analyze the variation of the term $\left|\frac{1}{1+j\lambda_n}\right|$, rather than the variation of the isolated eigenvalue. This term is usually called the modal significance (*MS*), as it represents the normalized amplitude of the current modes [23]. This normalized amplitude only depends on the shape and size of the conducting object, and it does not account for excitation.

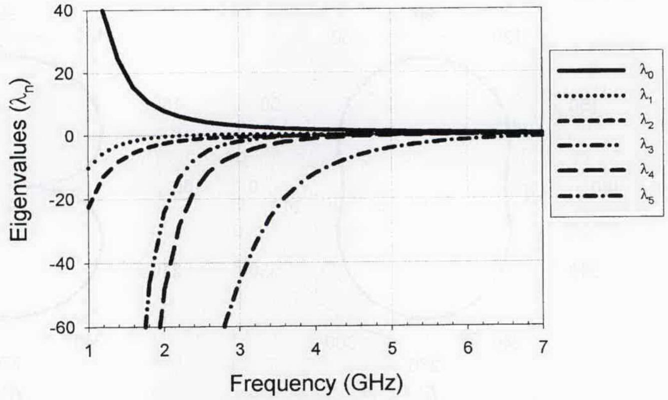

Figure 4. The variation with frequency of the eigenvalues, λ_n, associated to the current modes, J_n, of the rectangular plate depicted in Figure 1.

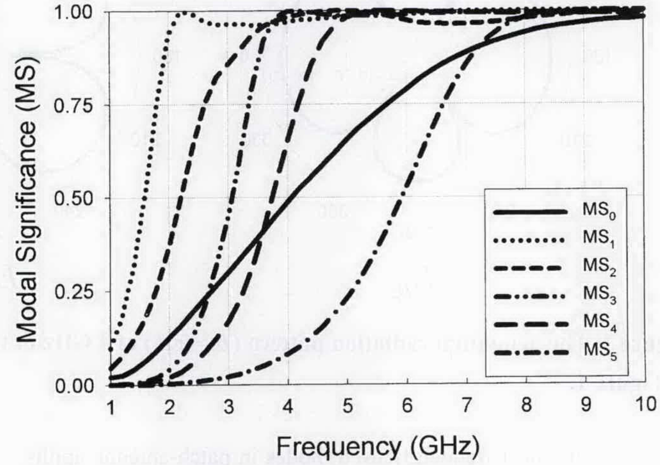

Figure 5. The variation with frequency of the modal significance (*MS*) related to the current modes J_n of Figure 1.

Figure 5 depicts the variation with frequency of the modal significance related to current modes J_n of the rectangular plate of Figure 1. The resonance of each mode can be identified by a maximum value of one in the modal-significance curves. This means that the nearer the curve is to its maximum value, the most effectively the associated mode contributes to radiation. The radiating bandwidth of a mode can then be established according to the width of its modal-significance curve near the maximum point. As shown in Figure 5, for the case of the rectangular plate of dimension 4 cm × 6 cm, all characteristic modes except for mode J_0 present quite efficient radiating behaviors, as their *MS* curves stand slightly below the maximum value of one, after resonance.

However, there exists another even-more-intuitive representation of the eigenvalues, which is based on the use of characteristic angles. Characteristic angles are defined in [30] as

$$\alpha_n = 180° - \tan^{-1}(\lambda_n). \quad (10)$$

From a physical point of view, the characteristic angle models the phase difference between a characteristic current, J_n, and the associated characteristic field, E_n. Figure 6 presents the variation with frequency of the characteristic angle, α_n, associated with the current modes of the rectangular plate of Figure 1. Observe that a mode resonates when $\lambda_n = 0$, that is, when its characteristic angle is $\alpha_n = 180°$. Therefore, when the characteristic angle is close to 180°, the mode is a good radiator. When the characteristic angle is near 90° or 270°, the mode mainly stores energy. Thus, the radiating bandwidth of a mode can be obtained from the slope at 180° of the curve described by the characteristic angles.

Although the information given by Figure 6 could have also been extracted from Figure 4 or Figure 5, the characteristic-angle representation is often preferred, as it is the most intuitive representation. From Figure 6, the resonance frequency of each mode can be easily identified by looking for the points where $\alpha_n = 180°$. Hence, mode J_1 resonates at 2.2 GHz, mode J_2 at 5 GHz, mode J_3 at 4.2 GHz, mode J_4 at 5.6 GHz, and mode J_5 at 10 GHz. The special nature of the nonresonant inductive mode, J_0, is also observed in Figure 6, since its associated angle remains below 180° at every frequency.

Finally, it should be emphasized that the modal study presented here for the rectangular plate could also have been performed for planar structures of any shape. It is worth mentioning that characteristic modes present quite a predictable behavior in planar structures, whatever is their shape. As an example, Figure 7 shows the normalized current distribution at 2.4 GHz of the first eigenvector, J_1, and the second eigenvector, J_2, of several planar geometries. From these results, it can be derived that the first eigenvector, J_1, is always characterized by a horizontal current flow, except for the contour where it follows the perimeter of the structures. Likewise, the second eigenvector, J_2, presents vertical currents along the different plates, with the exception of the contour.

4. Design Examples

This section is focused on presenting several antenna designs that have been achieved by direct application of the Theory of Characteristic Modes. Examples comprise a patch-antenna design, reflectarrays, a planar-monopole design, and the examination of a novel design concept for handset antennas.

4.1 Arbitrarily Shaped Microstrip Patches with Circular Polarization

It is a well-known fact that to get circular polarization from a microstrip patch, it is necessary to combine two orthogonal and linearly polarized modes, with the same current amplitude and in phase quadrature. The orthogonality properties of characteristic modes make the generation of circular polarization in arbitrary patches possible in an easy and intuitive way. For the sake of example, let us describe the procedure carried out to design a circularly polarized isosceles-triangular patch antenna using characteristic modes. The dimensions of this triangular patch are shown in Figure 8a. The current distribution at 3.4 GHz of the modes to be combined – which are the horizontal and the vertical current modes – is shown in Figure 8b. From the information provided by the modal-significance curves in Figure 9a, it can be determined that both modes present exactly the same current amplitude at 3.4 GHz. Moreover, from the characteristic-angle curves presented in Figure 9b, it can be derived that at 3.4 GHz, both modes present a 90° phase difference. Hence, if these two modes were properly excited and combined, they would yield circular polarization at 3.4 GHz. So, the next step is to identify where the feed point should be located to excite these modes.

Figure 10 shows the optimum feed position where the two modes present exactly the same current amplitude. This point corresponds to the minimum value obtained after subtracting the two current distributions in Figure 8b at 3.4 GHz. Last of all, the axial ratio plotted in Figure 11 – which was obtained by using an aperture feed with a 45° rotation located at the previously specified point – attests to the fact that the triangular patch is circularly polarized in the broadside direction at 3.4 GHz.

4.2 Optimization of the Polarization of Reflectarrays Using Characteristic Modes

Another interesting application of characteristic modes is to adjust the phase of the field reflected by the individual elements of a reflectarray antenna [31]. As described in [14], the eigenvalues, λ_n, are related to the scattering coefficient, S_n, by

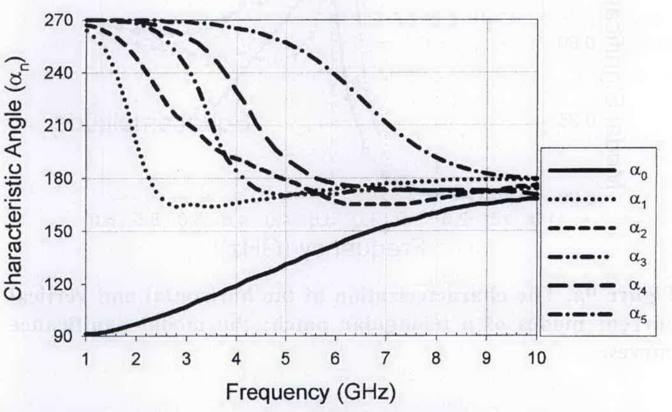

Figure 6. The variation with frequency of the characteristic angle, α_n, associated with the current modes of the rectangular plate in Figure 1.

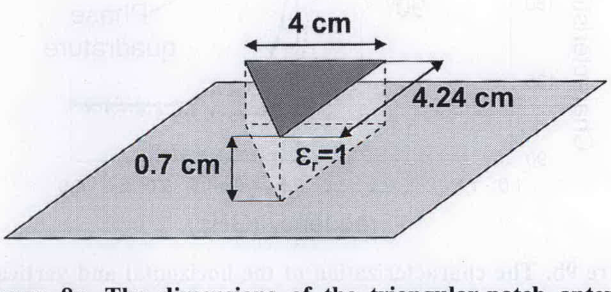

Figure 8a. The dimensions of the triangular-patch antenna placed over an infinite ground plane with air dielectric.

$$S_n = \frac{1 - j\lambda_n}{1 + j\lambda_n}. \qquad (11)$$

Then, the reflection phase of the nth mode can be expressed as

$$\varphi_n = -2\tan^{-1}(\lambda_n). \qquad (12)$$

Since Equation (12) does not depend on the excitation, when considering the illuminating feed the total reflection phase will be a combination of the reflection phases of the excited modes.

Typically, square and rectangular patches are the most widely used elements for reflectarray applications, due to their simplicity. However, they do not always provide the desired bandwidth performance. Recently, the use of ridges has been proposed in order to improve the bandwidth performance of rectangular patches [32]. However, this solution degrades the cross-polarization level, especially for the case of oblique incidence. In general, a square patch excited by an obliquely incident plane wave presents currents on its surface flowing in a diagonal direction. Figure 12a shows the current distribution at 8 GHz generated by a ϕ-polarized incident plane wave in the direction $\theta = 30°$ and $\phi = 45°$ over a square patch of dimension 15 mm, placed 3 mm above an infinite ground plane. This current flows in a diagonal direction ($-45°$) because of the excitation of two orthogonal degenerated modes: The vertical current mode (Figure 12b), and the horizontal current mode (Figure 12c). The radiation patterns at 8 GHz, due to the total current, in the x-z and y-z planes are plotted in Figure 13. As a result of the excitation of the two degenerated modes, the theta and phi components of the electric field are present in both planes.

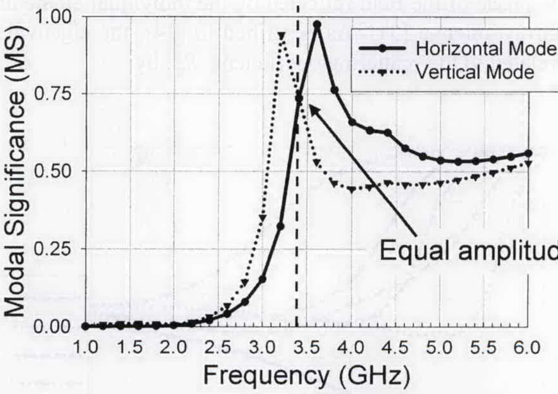

Figure 9a. The characterization of the horizontal and vertical current modes of a triangular patch: the modal-significance curves.

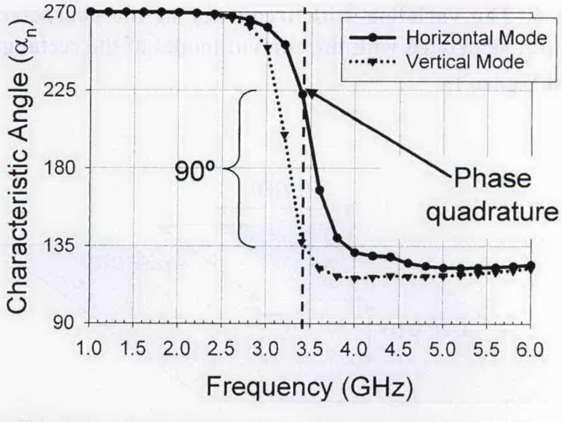

Figure 9b. The characterization of the horizontal and vertical current modes of a triangular patch: the characteristic angle variation with frequency.

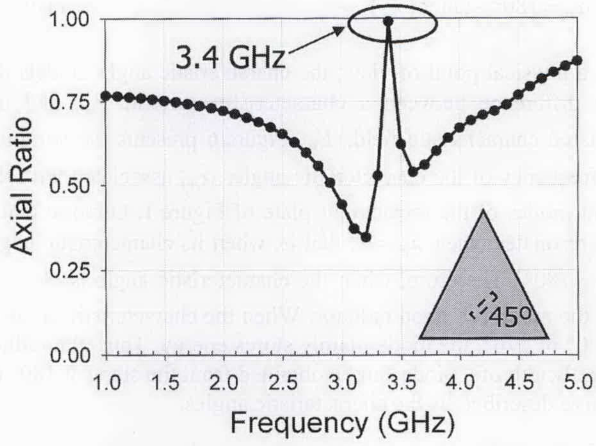

Figure 11a. The axial ratio for the broadside direction for an aperture-coupled feed at 45°.

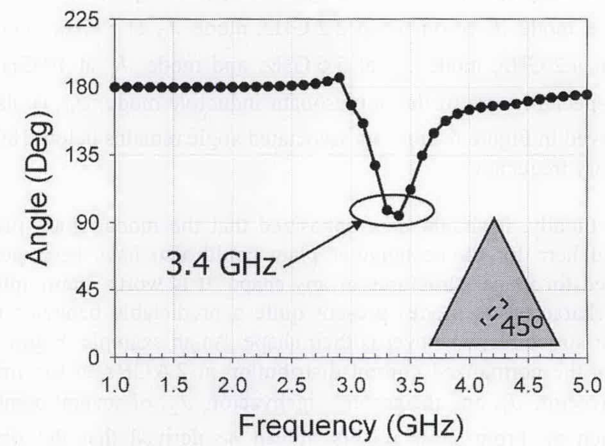

Figure 11b. The phase difference for the broadside direction for an aperture-coupled feed at 45°.

One solution to improve the polarization purity of the square patch for the case of oblique incidence is to split the degenerated modes, so that only one of them is excited at the desired frequency. This can be accomplished just by dividing the patch in two rectangular strips along the direction of the desired polarization [33]. Figure 14 illustrates the normalized current distribution at 8 GHz for the first three modes of the square patch divided into two vertical strips. When the square is divided along the y-axis direction the vertical mode is preserved, while the horizontal mode in Figure 14, the current of which is interrupted by the gap, resonates at a higher frequency. Additionally, a new vertical mode also appears, with currents flowing with opposite phase in the strips. Figure 15 shows curves of the reflection phase as a function of frequency associated with the aforementioned modes of the two vertical strips. This reflection phase was obtained using Equation (12). For the sake of comparison, Figure 15 also includes the reflection phase of the vertical mode of the square patch. From Figure 15, it can be determined that the vertical-current mode of the two vertical strips presents the same reflection phase as the vertical mode of the com-

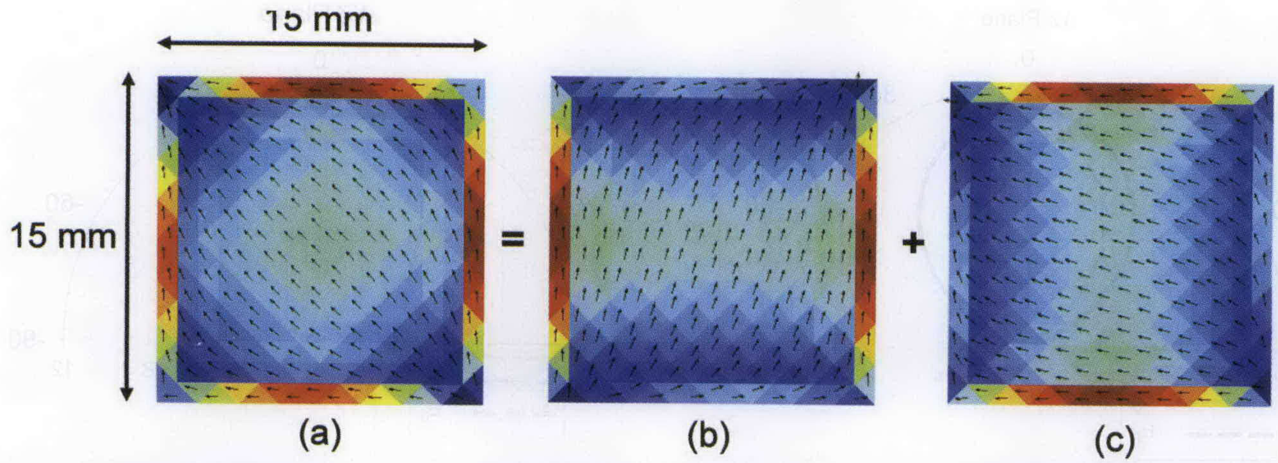

Figure 12. (a) The total current at 8 GHz for a square patch when excited by a ϕ-polarized incident plane wave ($\theta = 30°$, $\phi = 45°$); (b) The vertical current mode at 8 GHz; (c) The horizontal current mode at 8 GHz.

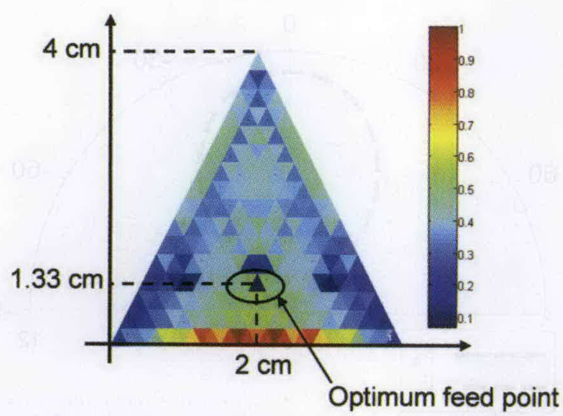

Figure 10. The optimum feed position to obtain circular polarization in a triangular patch.

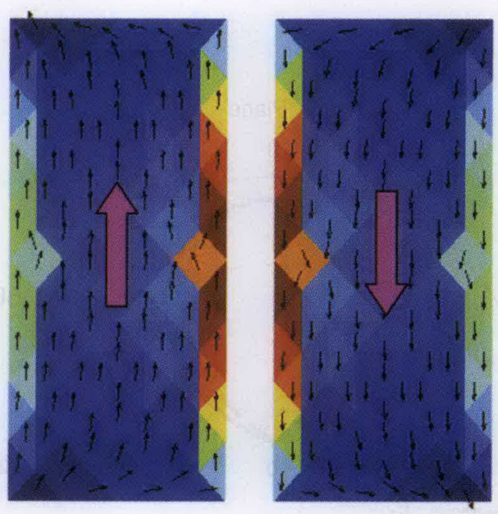

Figure 14b. The normalized current distribution at 8 GHz for the vertical current mode with currents flowing in the opposite way for two vertical strips placed 3 mm above an infinite ground plane.

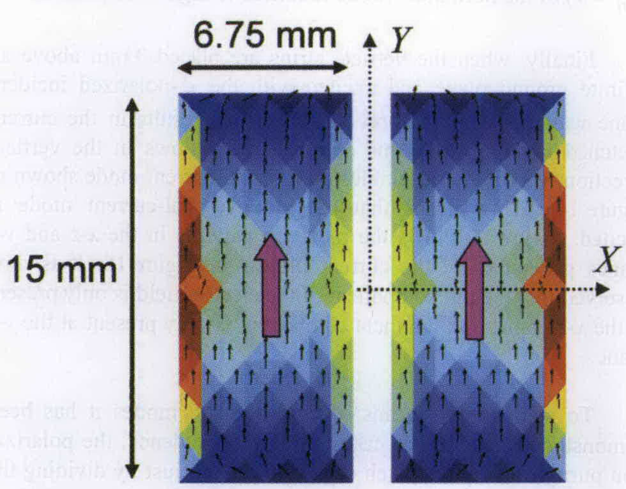

Figure 14a. The normalized current distribution at 8 GHz for the vertical current mode of two vertical strips placed 3 mm above an infinite ground plane.

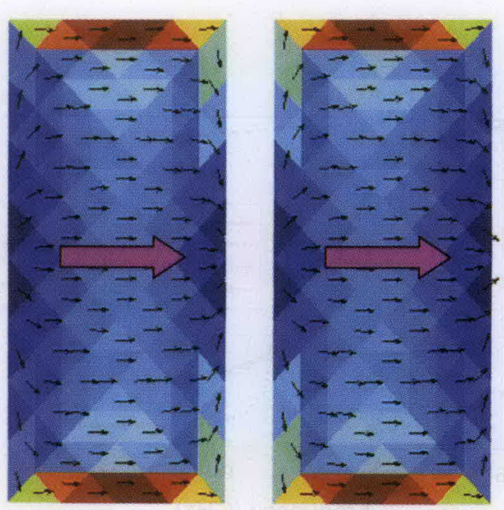

Figure 14c. The normalized current distribution at 8 GHz for the horizontal current mode of two vertical strips placed 3 mm above an infinite ground plane.

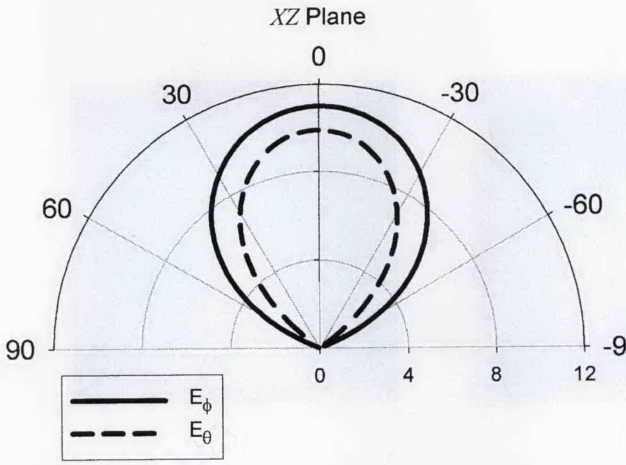

Figure 13a. The *x-z* plane radiation pattern at 8 GHz due to the diagonal current plotted in Figure 12.

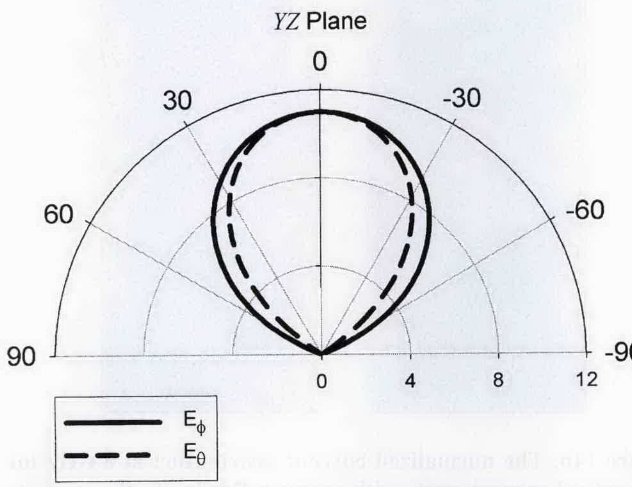

Figure 13a. The *y-z* plane radiation pattern at 8 GHz due to the diagonal current plotted in Figure 12.

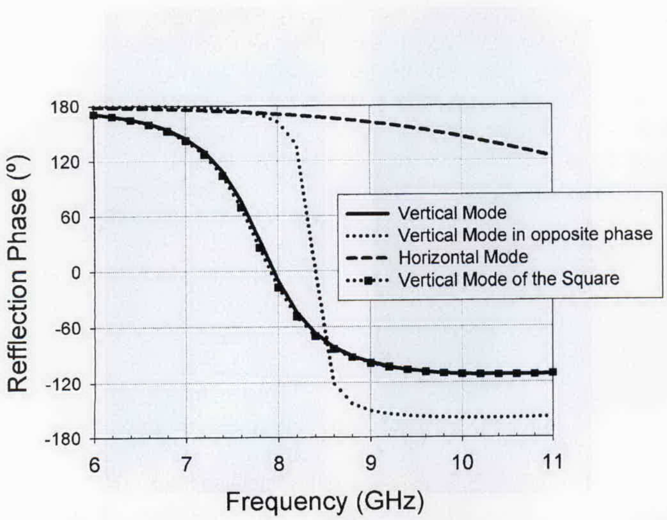

Figure 15. The reflection phase as a function of frequency for the modes of the two vertical strips, and for the vertical mode of the square patch.

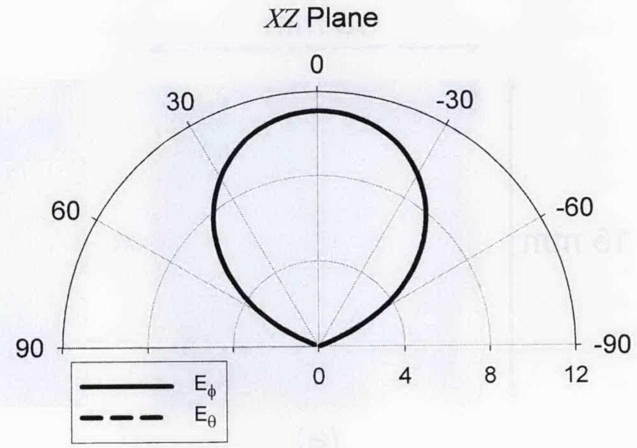

Figure 17a. The *x-z* plane radiation pattern generated by the current plotted in Figure 16.

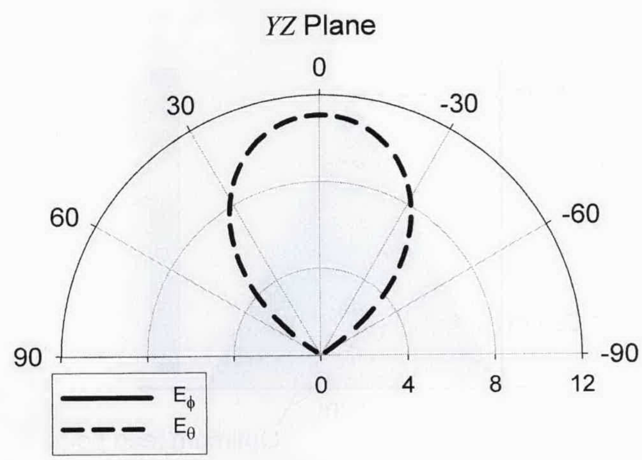

Figure 17b. The *y-z* plane radiation pattern generated by the current plotted in Figure 16.

plete square patch. It can also be determined that the resonance ($\varphi_n = 0$) of the horizontal mode is shifted to higher frequencies.

Finally, when the vertical strips are placed 3 mm above an infinite ground plane and excited with the ϕ-polarized incident plane wave used in the previous case, this results in the current sketched in Figure 16. This current, which flows in the vertical direction, very much resembles the vertical-current mode shown in Figure 14a. This means that only the vertical-current mode is excited. Figure 17 shows the radiation patterns in the *x-z* and *y-z* planes generated by the current plotted in Figure 16. It is now observed that the phi component of the electric field is only present at the *x-z* plane, and the theta component is only present at the *y-z* plane.

To sum up, by means of characteristic modes it has been demonstrated that for the case of oblique incidence, the polarization purity of a square patch can be improved just by dividing the patch into two rectangular strips in the direction of the desired polarization. With this simple modification of the square patch, the bandwidth performance of the fundamental mode is preserved, while the cross-polar component is very much reduced.

4.3 Double-Fed Planar Monopole Antennas

Planar monopoles are very-well-known antennas that have long been used in mobile communications, due to their wide impedance bandwidths, omnidirectional radiation patterns, simple structures, and low cost. Among the different monopole geometries, the circular disk has been reported to yield maximum bandwidth [34]. Later, in [35] was shown that although the square monopole provided smaller bandwidth than the circular monopole, its radiation pattern suffered less degradation within the impedance bandwidth. Nonetheless, using characteristic modes it can be demonstrated that with a proper feeding configuration, the square monopole delivers approximately the same input bandwidth as the circular monopole, but with improved polarization purity.

Let us consider a square planar monopole, analyzed from the image-theory point of view. As shown in Figure 18a, the monopole can be modeled as a planar plate with two narrow slits that account for the feeding gap. In patch-antenna design, the insertion of narrow slits at the patch's nonradiating edges is a commonly used technique for obtaining compact antennas [5]. The slits force the current to meander, so the resonant frequency decreases. The main problem with this technique is that the current meandering results in a horizontal component of the current, which degrades the polarization and bandwidth of the antenna. With the aim of verifying this assessment, Figure 18 illustrates the current distribution at resonance of the vertical-current mode of a rectangular plate of dimensions 8.5 cm × 4 cm, with and without slits. The vertical-current mode of the structure with slits resonates at 1.3 GHz, and presents a horizontal current flow near the slits. In contrast, the vertical-current mode of the complete rectangular plate resonates at a higher frequency, 1.6 GHz, and displays pure vertical currents. Moreover, currents in the rectangular plate are much more intense than in the plate with slits, for the same color scale.

Let us continue studying the curves showing characteristic angle as a function of frequency depicted in Figure 19. These curves demonstrate that the vertical-current mode of the rectangular plate offers broader radiating bandwidth than the plate with slits, since its associated characteristic angle stands near 180° in a wider frequency range. From these results, it arises that the bandwidth performance of the square monopole would improve if only the existence of vertical currents were allowed. This can be accomplished using the double-fed configuration shown in Figure 20. This square monopole, already presented in [36], uses a feeding structure that consists of a splitting network connected to two symmetrical ports at the base of the monopole. The symmetry of the ports prevents the excitation of horizontal currents, and assures that only the dominant vertical-current mode is present in the structure. The square dimension of the monopole is $L = 4\,\text{cm}$. Full details of the rest of dimensions of the antenna are given in [36].

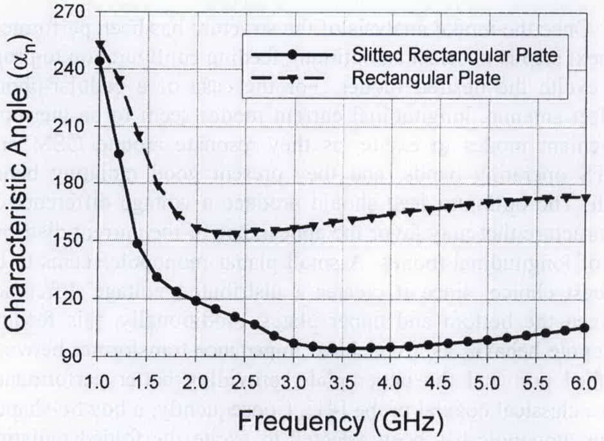

Figure 19. Curves of the characteristic angle as a function of frequency obtained for the rectangular plates presented in Figure 18.

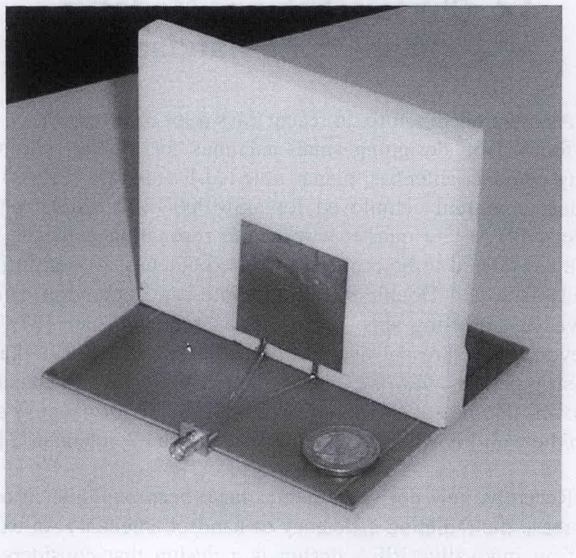

Figure 20. The prototype of the double-fed square monopole.

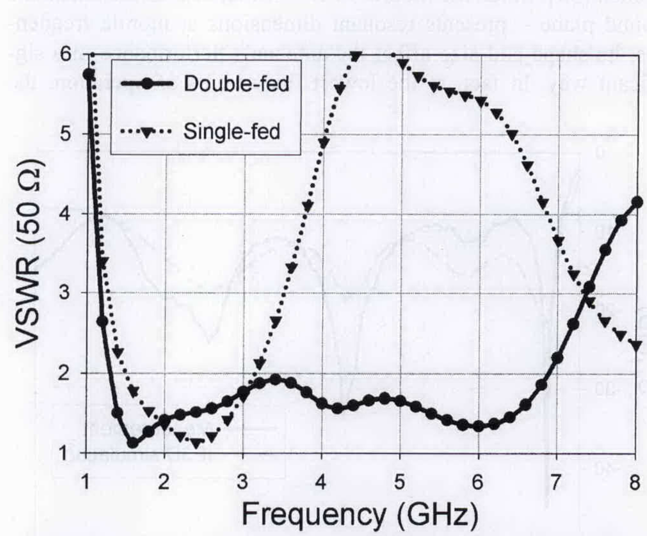

Figure 21. A comparison of the *VSWR* referred to 50 Ω of a double-fed square monopole and a single-fed square monopole of the same dimension.

To conclude this section, Figure 21 compares the voltage-standing-wave ratio (*VSWR*) of the double-fed square monopole to that of a single-fed square monopole of the same dimension. These results for the *VSWR* were obtained using the commercial electromagnetic software from Zeland, *IE3D*. As it was expected from the previous discussion, when using a double-feed configuration, the impedance bandwidth of the square monopole was greatly improved. Figure 22 reveals that simulated and measured results for the return loss of the prototype were in good agreement. For brevity, a demonstration of the reduction of the cross-polar component of the radiation pattern for the double-fed square monopole has not been included, yet it can be found in [36].

4.4 Chassis-Antenna Modes in Cellular-Phone Handsets

As mentioned before, in recent days a lot of investigation has been focused on designing small antennas for mobile terminals. Among compact antennas, planar inverted-F antennas (PIFAs) are the most commonly employed for GSM900/1800 cellular-phone handsets. PIFAs are quarter-wavelength resonating antennas that can be considered to be probe-fed shorted patches over an infinite ground plane [5]. Double-band and triple-band operation can be achieved by inserting slits in the PIFA's radiating path [37, 38]. However, PIFAs present two main drawbacks. The first is that as microstrip patches, they are inherently narrow-bandwidth antennas. Moreover, because of their compactness, their performance is subject to the well-known fundamental limits on small antennas [3].

Recently, new design strategies have been explored in order to increase the radiation efficiency of handset antennas. An example of an innovative PIFA design is a design that considers the printed-circuit board (PCB) of the mobile unit as part of the antenna [39]. Since the mobile PCB – which acts as the antenna's ground plane – presents resonant dimensions at mobile frequencies, its shape and size affect the antenna's performance in a significant way. In fact, at the lowest frequencies of operation, the PCB is the main radiator, while the antenna only works as a probe to excite the PCB's current modes. Obviously, to design an antenna from this new perspective, an in-depth knowledge of the current modes of the structure is needed. To that purpose, the Theory of Characteristic Modes may be very helpful [40].

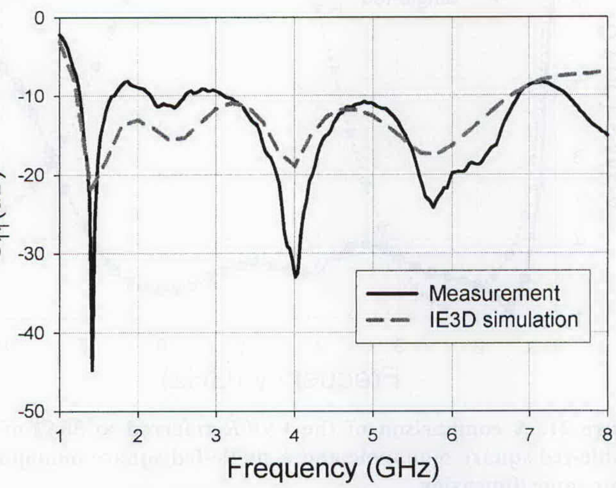

Figure 22. A comparison of simulated and measured results for the return loss referred to 50 Ω of the antenna prototype in Figure 20.

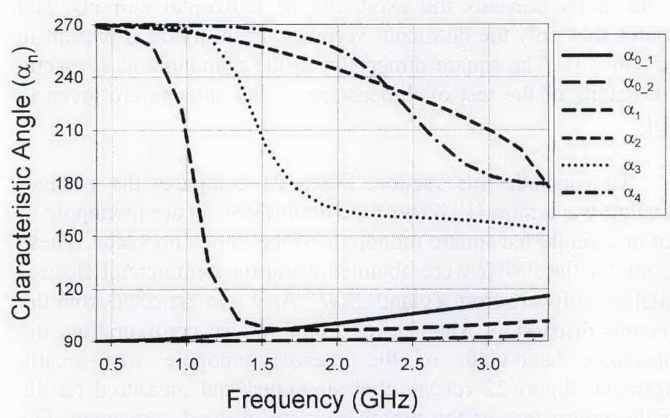

Figure 24. The characteristic angle variation with frequency for the first six characteristic modes of the folded radiating ground plane.

The next example shows the procedure carried out to design a handset antenna using the Theory of Characteristic Modes. Figure 23 shows the normalized current distribution at the first resonance (1.1 GHz) for the first six characteristic modes of the antenna, which is based on the PCB-resonance design concept. The antenna can be considered either as a PIFA over a finite ground plane, or as a folded radiating ground plane. The dimensions of the antenna are $L = 100$ mm, $W = 40$ mm, $W_s = 35$ mm, $h = 10$ mm, and $L_1 = 49.15$ mm. Note that dimensions L and W coincide approximately with the length and width of the PCB of a common mobile telephone. Arrows have been plotted together with characteristic currents for a better understanding of the current flow. As depicted in Figure 23, there are two modes, J_{01} and J_{02}, with currents forming closed loops. It will be verified later, with the information given by characteristic angles, that modes J_{01} and J_{02} are special nonresonant modes. Other modes, such as J_1, J_3, and J_4, exhibit longitudinal currents along the structure. Mode J_1 is the fundamental mode, and it flows uninterrupted from the open end on the upper plate to the open end on the lower plate. This fundamental mode resonates when the current path is approximately a half wavelength, and it is a folded version of mode J_1 in Figure 1. Modes J_3 and J_4 are higher-order longitudinal modes, which present one current null and two current nulls along the structure, respectively. Finally, mode J_2 is the only mode that presents transverse currents.

The resonance frequency and radiating bandwidth of the above-described current modes can be obtained from characteristic angles. Figure 24 plots characteristic angles associated with the current modes in Figure 23 as a function of frequency. It is observed that modes J_{01} and J_{02} do not resonate, and present an inductive contribution at every frequency. Longitudinal-current modes J_1, J_3, and J_4 resonate at 1.1 GHz, 1.7 GHz, and 3.25 GHz, respectively, while the transverse mode, J_2, resonates at 3.35 GHz. With regard to radiating bandwidth, the poorest radiating mode is J_1, since it exhibits the characteristic-angle curve with the steepest slope at 180°.

Once the modal analysis of the structure has been performed, the next step is to select an optimum feeding configuration to properly excite the desired modes. For the case of a cellular-phone handset antenna, longitudinal current modes seem to be the most convenient modes to excite, as they resonate around GSM and UMTS operating bands, and they present good radiating bandwidth. The optimum feed should produce a voltage difference in the structure that may favor the appearance of the current distribution of longitudinal modes. A small planar monopole seems to be the best choice, since it creates a distributed voltage difference between the bottom and upper plates. Additionally, this feeding monopole behaves as a wideband impedance transformer between the feed port and the upper plate, providing better performance than a classical coaxial probe [41]. Consequently, a bowtie-shaped planar monopole has been selected to excite the folded radiating ground plane. The monopole is bowtie in shape rather than rectangular or square because the bowtie has more parameters to adjust, and it is therefore easier to achieve maximum matching using this

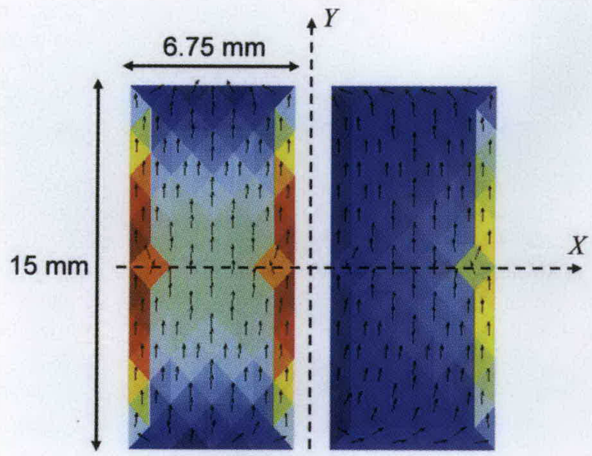

Figure 16. The total current at 8 GHz for two vertical strips when excited by a ϕ-polarized incident plane wave in the direction $\theta = 30°$, $\phi = 45°$.

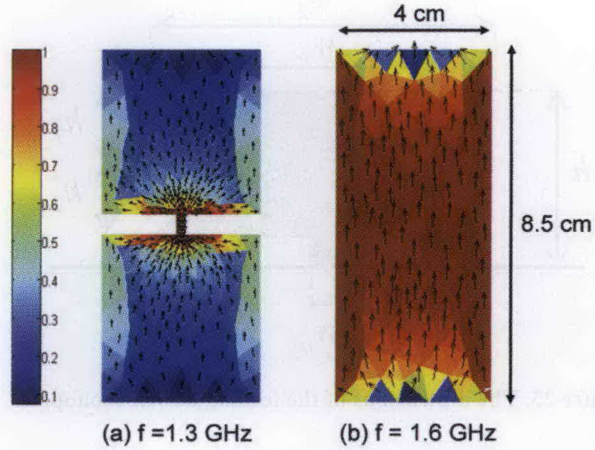

Figure 18. The current distribution at resonance for the vertical current mode of a rectangular plate of dimensions 8.5 cm × 4 cm: (a) with slits; (b) without slits.

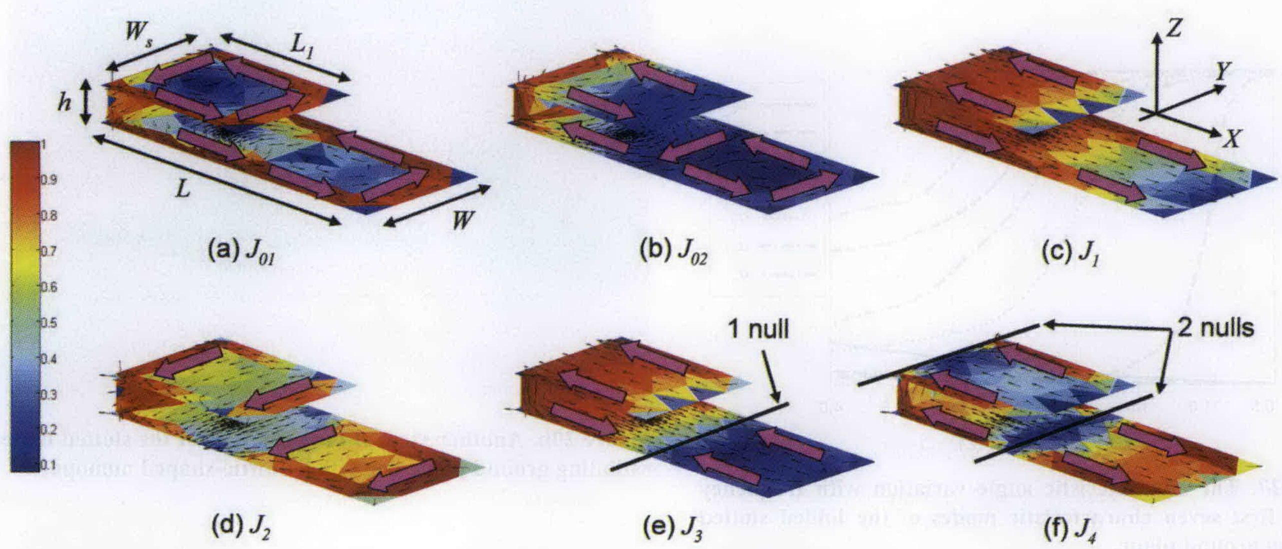

Figure 23. The normalized current distribution at the first resonance ($f = 1.1$ GHz) of the first six characteristic modes J_n of a folded radiating ground plane.

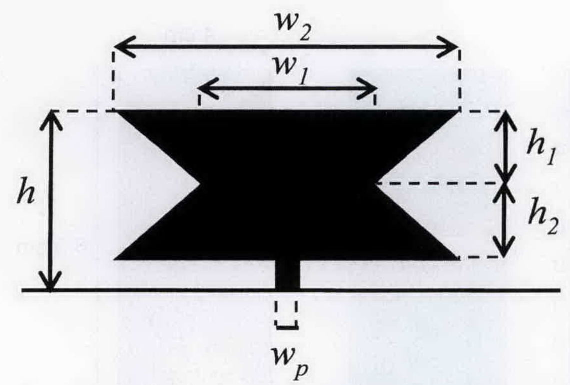

Figure 25. The dimensions of the feeding bowtie monopole.

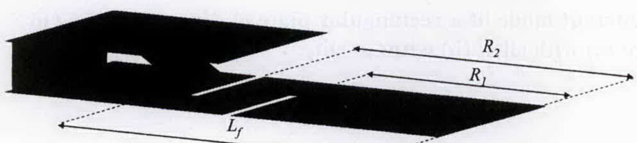

Figure 26. The geometry of the folded radiating ground plane with a bowtie-shaped feeding monopole.

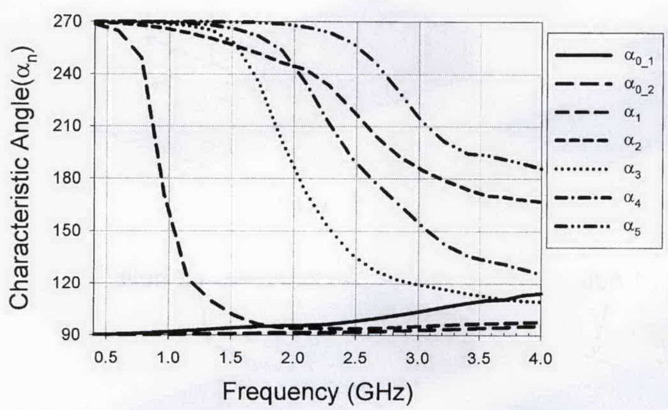

Figure 27. The characteristic angle variation with frequency for the first seven characteristic modes of the folded slotted radiating ground plane.

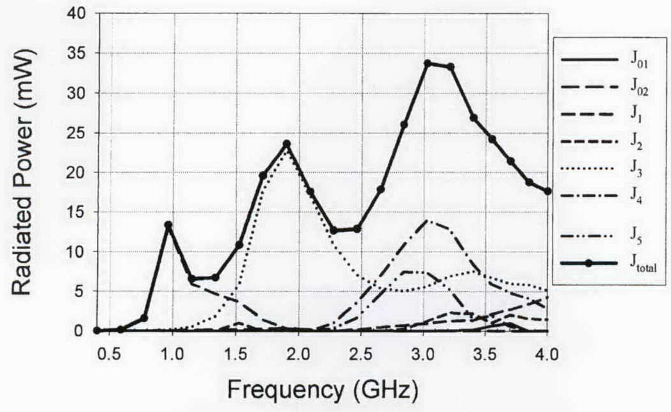

Figure 28. The contribution of the different modes to the total power radiated by the antenna.

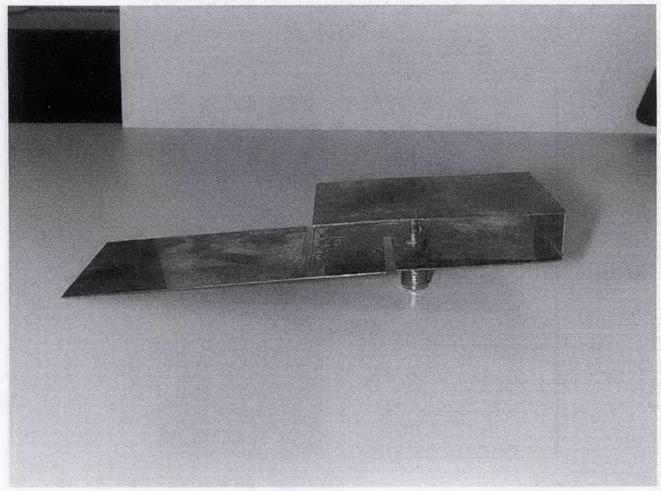

Figure 29a. The prototype of the slotted folded radiating ground plane fed with a bowtie-shaped monopole.

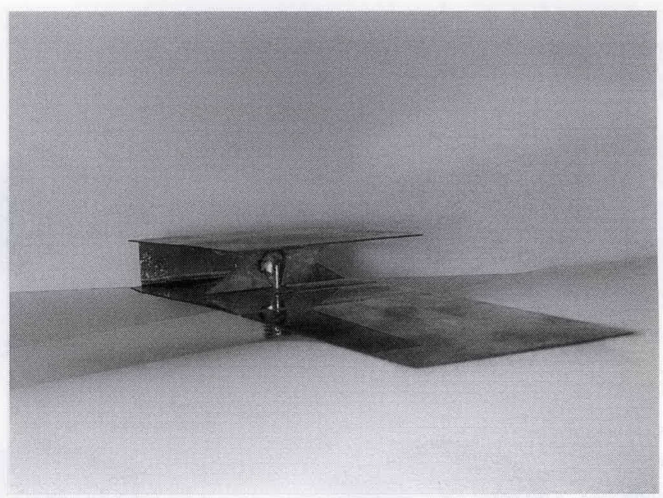

Figure 29b. Another view of the prototype of the slotted folded radiating ground plane fed with a bowtie-shaped monopole.

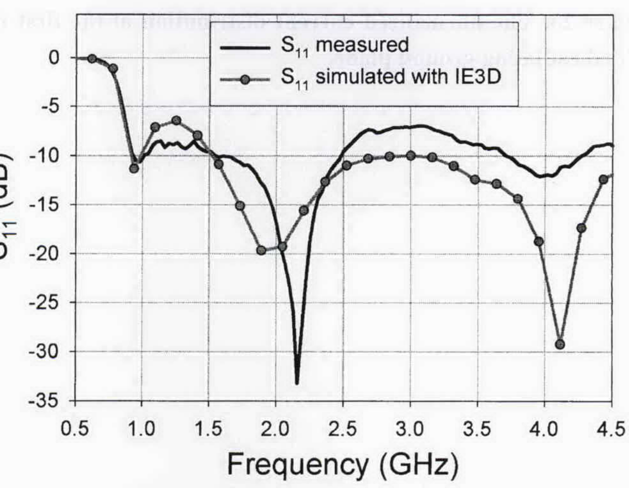

Figure 30. The simulated and measured return loss for the antenna prototype in Figure 29.

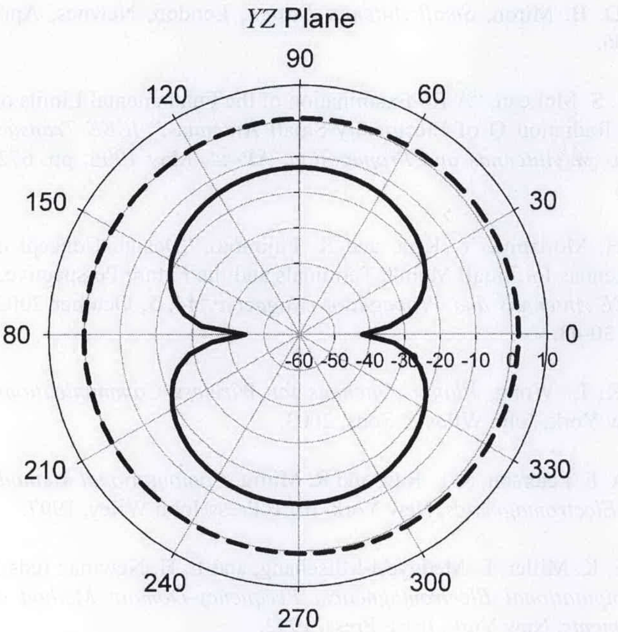

Figure 31a. The radiation pattern in the *y-z* plane for the slotted folded radiating ground plane at 900 MHz (solid line: E_θ; dashed line: E_ϕ).

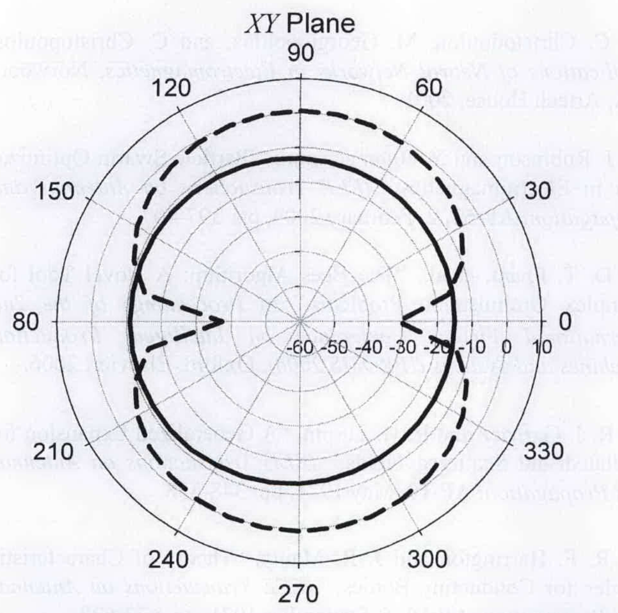

Figure 31b. The radiation pattern in the *x-y* plane for the slotted folded radiating ground plane at 900 MHz (solid line: E_θ; dashed line: E_ϕ).

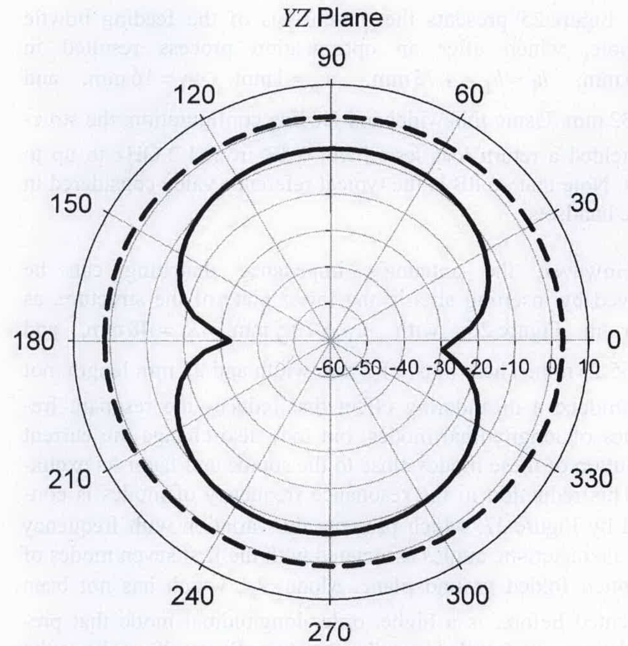

Figure 31c. The radiation pattern in the *y-z* plane for the slotted folded radiating ground plane at 1800 MHz (solid line: E_θ; dashed line: E_ϕ).

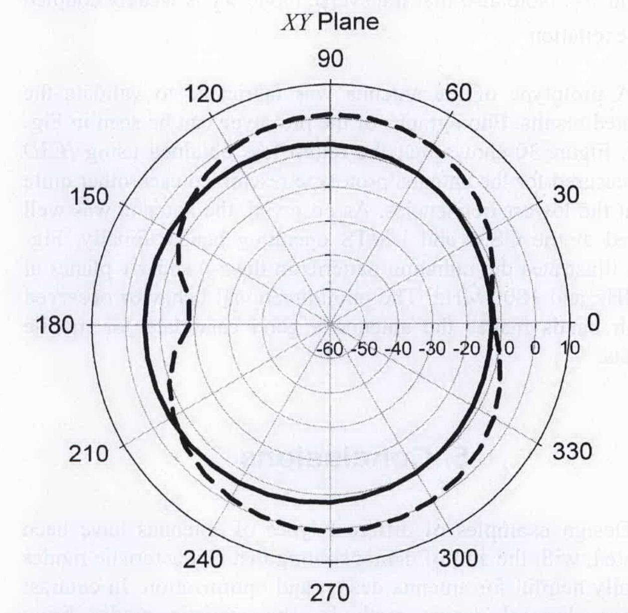

Figure 31d. The radiation pattern in the *x-y* plane for the slotted folded radiating ground plane at 1800 MHz (solid line: E_θ; dashed line: E_ϕ).

shape. Figure 25 presents the dimensions of the feeding bowtie monopole, which after an optimization process resulted in $h = 10$ mm, $h_1 = h_2 = 4.75$ mm, $w_p = 1$ mm, $w_l = 16$ mm, and $w_2 = 32$ mm. Using this wideband feeding configuration, the structure yielded a return loss less than –6 dB from 1.2 GHz to up to 6 GHz. Note that –6 dB is the typical reference value considered in mobile handsets.

However, the antenna's impedance matching can be improved by inserting slits in the lower plate of the structure, as shown in Figure 26, with $L_f = 72.5$ mm, $R_1 = 48$ mm, and $R_2 = 65.25$ mm. These slits, of 2 mm width and 25 mm length, not only produce a meandering effect that reduces the resonant frequencies of longitudinal modes, but they also change the current distribution of these modes close to the source and favor its excitation. This reduction in the resonance frequency of modes is confirmed by Figure 27, which presents the variation with frequency of the characteristic angles associated with the first seven modes of the slotted folded ground plane. Mode J_5, which has not been represented before, is a higher-order longitudinal mode that presents three current nulls along the structure. Figure 28 analyzes the contribution of each mode to the total power radiated by the antenna. Note that the first power maximum, approximately at 0.9 GHz, is caused by mode J_1; the second maximum, at 1.8 GHz, is due to the excitation of mode J_3; and the third maximum, at 3.2 GHz, results from the contribution of longitudinal modes J_3, J_4, and J_5. Note also that transverse mode J_2 is weakly coupled to the excitation.

A prototype of the antenna was fabricated to validate the simulated results. Photographs of the prototype can be seen in Figure 29. Figure 30 shows that the return loss obtained using *IE3D* and measured for the antenna prototype resembled each other quite a lot at the lowest frequencies. As observed, the antenna was well matched at the GSM and UMTS operating bands. Finally, Figure 31 illustrates the radiation patterns in the *z-y* and *x-y* planes at 900 MHz and 1800 MHz. The omnidirectional behavior observed in both bands makes the antenna a good candidate for mobile handsets.

5. Conclusions

Design examples of different types of antennas have been presented, with the aim of demonstrating that characteristic modes are really helpful for antenna design and optimization. In contrast to other classical design methods, characteristic modes bring physical insight into the radiating behavior of the antenna, so a controlled design can be performed. The resonance frequencies of the modes, as well as their radiating behavior, can be determined from the information provided by eigenvalues. Moreover, having in mind the current distribution of the modes, the geometry of the antenna can be modified to accomplish the desired specifications, and an appropriate feeding configuration can be selected in order to excite the desired modes.

6. References

1. K. L. Wong, *Compact and Broadband Microstrip Antennas*, New York, John Wiley & Sons, 2002.

2. D. B. Miron, *Small Antenna Design*, London, Newnes, April 2006.

3. J. S. McLean, "A Re-Examination of the Fundamental Limits on the Radiation Q of Electrically Small Antennas," *IEEE Transactions on Antennas and Propagation*, **AP-44**, May 1996, pp. 672-676.

4. H. Morishita, Y. Kim, and K. Fujimoto, "Design Concept of Antennas for Small Mobile Terminals and the Future Perspective," *IEEE Antennas and Propagation Magazine*, **44**, 5, October 2002, pp. 30-43.

5. K. L. Wong, *Planar Antennas for Wireless Communications*, New York, John Wiley & Sons, 2003.

6. A. F. Peterson, S. L. Ray, and R. Mittra, *Computational Methods for Electromagnetics*, New York, IEEE Press/John Wiley, 1997.

7. E. K. Miller, L. Medgyesi-Mitschang, and E. H. Newman (eds.), *Computational Electromagnetics: Frequency-Domain Method of Moments*, New York, IEEE Press, 1992.

8. E. K. P. Chong and S. H. Zak, *An Introduction to Optimization*, New York, John Wiley & Sons, 2001.

9. Y. Rahmat-Samii and E. Michielssen, *Electromagnetic Optimization by Genetic Algorithms*, New York, John Wiley & Sons, 1999.

10. C. Christodoulou, M. Georgiopoulos, and C. Christopoulos, *Applications of Neural Networks in Electromagnetics*, Norwood, MA, Artech House, 2001.

11. J. Robinson and Y. Rahmat-Samii, "Particle Swarm Optimization in Electromagnetics," *IEEE Transactions on Antennas and Propagation*, **AP-52**, 2, February 2004, pp. 397-407.

12. D. T. Pham, et al., "The Bees Algorithm: A Novel Tool for Complex Optimisation Problems," in *Proceedings of the 2nd International Virtual Conference on Intelligent Production Machines and Systems (IPROMS 2006)*, Oxford, Elsevier, 2006.

13. R. J. Garbacz and R. H. Turpin, "A Generalized Expansion for Radiated and Scattered Fields," *IEEE Transactions on Antennas and Propagation*, **AP-19**, May 1971, pp. 348-358.

14. R. F. Harrington and J. R. Mautz, "Theory of Characteristic Modes for Conducting Bodies," *IEEE Transactions on Antennas and Propagation*, **AP-19**, 5, September 1971, pp. 622-628.

15. R. F. Harrington and J. R. Mautz, "Computation of Characteristic Modes for Conducting Bodies," *IEEE Transactions on Antennas and Propagation*, **AP-19**, 5, September 1971, pp. 629-639.

16. R. J. Garbacz and D. M. Pozar, "Antenna Shape Synthesis Using Characteristic Modes," *IEEE Transactions on Antennas and Propagation*, **AP-30**, 3, May 1982, pp. 340-350.

17. D. Liu, R. J. Garbacz, and D. M. Pozar, "Antenna Synthesis and Optimization Using Generalized Characteristic Modes," *IEEE Transactions on Antennas and Propagation*, **AP-38**, 6, June 1990, pp. 862-868.

18. R. F. Harrington and J. R. Mautz, "Control of Radar Scattering by Reactive Loading," *IEEE Transactions on Antennas and Propagation*, **AP-20**, 4, July 1972, pp. 446-454.

19. A. El-Hajj, K. Y. Kabalan, and R. F. Harrington "Characteristic Modes of a Slot in a Conducting Cylinder and their Use for Penetration and Scattering, TE Case," *IEEE Transactions on Antennas and Propagation*, **AP-40**, 2, February 1992, pp. 156-161.

20. A. El-Hajj, and K. Y. Kabalan, "Characteristic Modes of a Rectangular Aperture in a Perfectly Conducting Plane," *IEEE Transactions on Antennas and Propagation*, **AP-42**, 10, October 1994, pp. 1447-1450.

21. R. F. Harrington and J. R. Mautz, "Pattern Synthesis for Loaded n-Port Scatterers," *IEEE Transactions on Antennas and Propagation*, **AP-22**, 2, March 1974, pp. 184-190.

22. J. R. Mautz and R. F. Harrington, "Radiation and Scattering from Bodies of Revolution," *Appl. Sci. Res.*, **20**, June 1969, pp. 405-435.

23. B. A. Austin and K. P. Murray, "The Application of Characteristic-Mode Techniques to Vehicle-Mounted NVIS Antennas," *IEEE Transactions on Antennas and Propagation*, **AP-40**, 1, February 1998, pp. 7-21.

24. R. F. Harrington, *Field computation by Moment Methods*, New York, MacMillan, 1968.

25. S. M. Rao, D. R. Wilton, and A. W. Glisson, "Electromagnetic Scattering by Surfaces of Arbitrary Shape," *IEEE Transactions on Antennas and Propagation*, **AP-30**, pp. 409-418, 1982.

26. Z. Bai, J. Demmel, J. Dongarra, A. Ruhe, and H. Van Der Vorst (eds.), *Templates for the Solution of Algebraic Eigenvalue Problems: A Practical Guide*, Philadelphia, SIAM (Society for Industrial and Applied Mathematics), 2000.

27. M. Cabedo, E. Antonino, M. Ferrando, and A. Valero, "On the Use of Characteristic Modes to Describe Patch Antenna Performance," 2003 International Symposium on Antennas and Propagation and URSI North American Radio Science Meeting, Columbus, Ohio, June 2003.

28. M. Cabedo, A. Valero, J. I. Herranz, and M. Ferrando, "A Discussion on the Characteristic Mode Theory Limitations and its Improvements for the Effective Modeling of Antennas and Arrays," 2004 International Symposium on Antennas and Propagation and USNC/URSI National Radio Science Meeting, Monterey, California, July 2004.

29. E. Suter and J. R. Mosig, "A Subdomain Multilevel Approach for the Efficient MoM Analysis of Large Planar Antennas," *Microwave and Optical Technology Letters*, **26**, 4, August 2000, pp. 270-277.

30. E. H. Newman, "Small Antenna Location Synthesis Using Characteristic Modes," *IEEE Transactions on Antennas and Propagation*, **AP-21**, 6, November 1973, pp. 868-871.

31. R. E. Munson, H. Haddad, and J. Hanlen, *Microstrip Reflectarray Antenna for Satellite Communication and RCS Enhancement or Reduction*, US Patent No. 4684952, 1987.

32. M. Bozzi, S. Germani, and L. Perregrini, "Performance Comparison of Different Element Shapes Used in Printed Reflectarrays," *Antennas and Wireless Propagation Letters*, **2**, 2003, pp. 219-222.

33. M. Cabedo, E. Antonino, A. Valero and M. Ferrando, "Optimization of the Polarization of Reflectarrays Using Characteristic Modes," 2004 International Symposium on Antennas and Propagation and USNC/URSI National Radio Science Meeting, Monterey, California, July 2004.

34. N. P. Agrawall, G. Kumar, and K. P. Ray, "Wide-Band Planar Monopole Antennas," *IEEE Transactions on Antennas and Propagation*, **AP-46**, February 1998, pp. 294-295.

35. M. J. Ammann, "Impedance Bandwidth of the Square Planar Monopole," *Microwave Opt. Technol. Lett.*, **24**, 3, February 2000, pp. 185-187.

36. E. Antonino-Daviu, M. Cabedo-Fabrés, M. Ferrando-Bataller, and A. Valero-Nogueira, "Wideband Double-Fed Planar Monopole Antennas," *Electronics Letters*, **39**, 23, November 2003, pp. 1635-1636.

37. Z. D. Liu, P. S. Hall, and D. Wake, "Dual Frequency Planar Inverted-F Antenna," *IEEE Transactions on Antennas and Propagation*, **AP-45**, October 1997, pp. 1451-1458.

38. W. P. Dou and Y. W. M. Chia, "Novel Meandered Planar Inverted-F Antennas for Triple Frequency Operation," *Microwave and Opt. Technol. Lett.*, **27**, October 2000, pp. 58-60.

39. P. Vainikainen, J. Ollikainen, O. Kivekas, and I. Kelander, "Resonator-Based Analysis of the Combination of Mobile Handset Antenna and Chassis," *IEEE Transactions on Antennas and Propagation*, **AP-50**, 10, October 2002, pp. 1433-1444.

40. E. Antonino-Daviu, C. A. Suarez-Fajardo, M. Cabedo-Fabrés, and M. Ferrando-Bataller, "Wideband Antenna for Mobile Terminals Based on the Handset PCB Resonance," *Microwave Opt. Technol. Lett.*, **48**, 7, July 2006, pp. 1408-1411.

41. Z. N. Chen and M. Y. W. Chia, "A Feeding Scheme for Enhancing the Impedance Bandwidth of a Suspended Plate Antenna," *Microwave Opt. Technol. Lett.*, **38**, 2003, pp. 21-25.

Introducing the Feature Article Authors

Marta Cabedo was born in Valencia, Spain, on June 8, 1976. She received the MS degree in Electrical Engineering from Universidad Politecnica de Valencia, Spain, in 2001.

In 2001, she joined the Electromagnetic Radiation Group at Universidad Politécnica de Valencia (UPV), as a Research Assistant, where she is currently finishing the PhD degree. In 2004, she became an Associate Professor in the Communications Department, Universidad Politecnica de Valencia. Her current scientific interests include numerical methods for solving electromagnetic problems, and design and optimization techniques for wideband and multi-band antennas.

Eva Antonino was born in Valencia, Spain, on July 1978. She received the MS degree in Electrical Engineering from the Universidad Politecnica de Valencia, Spain, in 2002.

In 2002, she joined the Electromagnetic Radiation Group, Universidad Politecnica de Valencia, where she is currently pursuing her PhD degree. In 2005, she became an Assistant Professor in the Communications Department, Universidad Politecnica de Valencia. In 2005, she stayed for several months as a visiting researcher at IMST GMbH in Kamp-Lintfort, Germany. Her research interests include wideband and multi-band planar antenna design and optimization, and computational methods for printed structures.

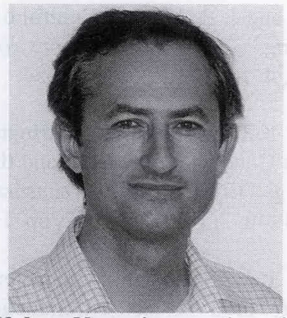

Alejandro Valero-Nogueira was born in Madrid, Spain, on July 19, 1965. He received the MS degree in Electrical Engineering from Universidad Politecnica de Madrid, Madrid, Spain, in 1991, and the PhD degree in Electrical Engineering from Universidad Politécnica de Valencia, Valencia, Spain in 1997.

In 1992, he joined the Departamento de Comunicaciones, Universidad Politécnica de Valencia, where he is currently an Associate Professor. During 1999, he was on leave at the ElectroScience Laboratory, The Ohio State University, Columbus, where he was involved in fast solution methods in electromagnetics and conformal antenna arrays. His current research interests include computational electromagnetics, Green's functions, waveguide slot arrays, and automated antenna-design procedures.

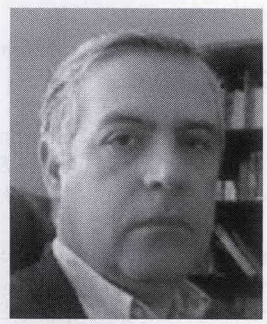

Miguel Ferrando-Bataller was born in Alcoy, Spain, in 1954. He received the MS and PhD degrees in Electrical Engineering from the Universidad Politecnica de Catalunya, Barcelona, Spain, in 1977 and 1982, respectively.

From 1977 to 1982, he was a Teaching Assistant with the Antennas, Microwave, and Radar Group, Universidad Politecnica de Catalunya, and in 1982 he became an Associate Professor. In 1990, he joined the Universidad Politecnica de Valencia, Valencia, Spain, where he is a Professor. His current research activities include numerical methods, antenna design, and e-learning activities.